Journal Pre-proof

Bio-physical mechanisms of dehydrating membranes of *Acinetobacter baumannii* linked to drought-resistance

Elisa Fardelli, Massimiliano Lucidi, Michael Di Gioacchino, Shadi Bashiri, Luca Persichetti, Giulia Capecchi, Tecla Gasperi, Armida Sodo, Paolo Visca, Giovanni Capellini

PII: S0005-2736(22)00183-3
DOI: https://doi.org/10.1016/j.bbamem.2022.184045
Reference: BBAMEM 184045

To appear in: *BBA - Biomembranes*

Received date : 16 June 2022
Revised date : 29 July 2022
Accepted date : 5 September 2022

Please cite this article as: E. Fardelli, M. Lucidi, M. Di Gioacchino et al., Bio-physical mechanisms of dehydrating membranes of *Acinetobacter baumannii* linked to drought-resistance, *BBA - Biomembranes* (2022), doi: https://doi.org/10.1016/j.bbamem.2022.184045.

Graphical Abstract

Bio-physical mechanisms of dehydrating membranes of *Acinetobacter baumannii* linked to drought-resistance

Elisa Fardelli, Massimiliano Lucidi, Michael Di Gioacchino, Shadi Bashiri, Luca Persichetti, Giulia Capecchi, Tecla Gasperi, Armida Sodo, Paolo Visca, Giovanni Capellini

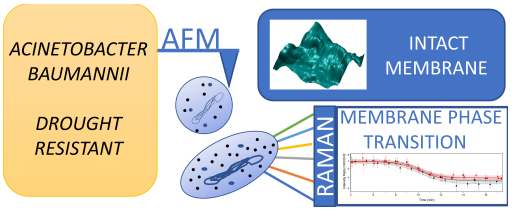

Highlights

Bio-physical mechanisms of dehydrating membranes of *Acinetobacter baumannii* linked to drought-resistance

Elisa Fardelli, Massimiliano Lucidi, Michael Di Gioacchino, Shadi Bashiri, Luca Persichetti, Giulia Capecchi, Tecla Gasperi, Armida Sodo, Paolo Visca, Giovanni Capellini

- *A. baumannii* is a hazardous nosocomial pathogen with a high dessication tollerance
- unknown bio-physical machanisms of *A. baumannii* to adapt to dehydration
- multi-technical investigation of bacterial cell membrane changes under dehydration
- decoupling of phase transitions and breakage of the membrane up to 24 h

Bio-physical mechanisms of dehydrating membranes of *Acinetobacter baumannii* linked to drought-resistance

Elisa Fardelli[a], Massimiliano Lucidi[a], Michael Di Gioacchino[a], Shadi Bashiri[b], Luca Persichetti[c], Giulia Capecchi[a], Tecla Gasperi[a,d], Armida Sodo[a], Paolo Visca[a,e], Giovanni Capellini[a]

[a] *University of Roma Tre, Department of Science, Viale G. Marconi, 446, Rome, 00146, Italy*
[b] *CNR, NEST, Istituto Nanoscienze, P.zza S. Silvestro, 12, Pisa, 56127, Italy*
[c] *University of Tor Vergata, Department of physics, Via della Ricerca Scientifica, 1, Rome, 00133, Italy*
[d] *National Institute of Biostructures and Biosystems (INBB), Viale delle Medaglie d'Oro, 305, Rome, 00136, Italy*
[e] *Santa Lucia Fundation IRCCS, Via dArdeatina, 306/354, Rome, 00179, Italy*

Abstract

Acinetobacter baumanni, is an opportunistic nosocomial multi-drug resistant bacterium, which represents a threat for human health. This pathogen is able to persist in intensive care units thanks to its extraordinary resistance towards dehydration, whose mechanisms are unknown and enable it to easily spread through surfaces, contaminating also medical devices. In this article we reveal, with a multimodal approach, based on μ–R Spectroscopy, Gas Chromatography coupled to Mass Spectroscopy, Atomic Force Microscopy and Fluorescence Recovery After Photobleaching, the bio-physical mechanisms that the membrane of two *A. baumannii* strains undergoes during dehydration. Showing a substantial decoupling of the phase transition from liquid crystalline to gel phase from evidence of cell lysis. Such decoupling may be the core of the resistance of *A. baumannii* against dehydration and highlights the different ability to resist to drought between strains.

Keywords:
Acinetobacter baumannii, AFM, Raman, membrane dehydration
PACS: 0000, 1111
2000 MSC: 0000, 1111

1. Introduction

In the last decades, battling hospitals-acquired infections has become a great challenge because of the emergence of drug-resistant pathogenic bacteria and their ability, not yet completely understood, to survive and persist in hospital environments, as for *Acinetobacter baumannii*. This Gram-negative bacterium is an opportunistic nosocomial pathogen responsible for a wide range of infections, such as bloodstream and urinary tract infections and ventilator-associated pneumonia (1). These infections are difficult to eradicate because multi-drug resistance runs in the genus (2), and because of the peculiar resistance against dehydration displayed by most of *A. baumannii* clinical isolates (2; 3). These features facilitate the contamination of life-support-machineries, such as mechanical ventilators, intravascular and urinary catheters, and drainage tubes, and contribute to the pathogen persistence in health care facilities. Unfortunately, the processes enabling its resistance to dehydration remain elusive.

Generally, during dehydration, both the lipopolysaccharides and phospholipids of the Gram-negative bacteria outer membrane undergo a phase transition from a liquid crystalline phase to a potentially deadly gel phase (4; 5; 6; 7). The first phase is a fluid healthy state with bent and loosely packed lipid chains, while in the gel phase, lipid chains are highly packed parallel to

each other, leading to stiffer membranes, which become rupture-prone and trigger the loss of cytoplasmatic content. During the transition from liquid crystal to gel phase, the Van der Waals' interactions between lipid chains and phase transition temperature, Tm, increase, along with the osmotic pressure that leads to a decrease in the membrane fluidity (7; 8). Thus, dry membranes are, preferentially, in a gel state at room temperature (depending on their composition). Once the cells are re-hydrated, Tm decreases and membranes undergo the reverse transition (4; 5; 6; 7; 8; 9; 10; 11).

In the specific case of *A. baumannii*, it is not clear whether its membrane experiences the phase transition and the resulting breakage. Thus, we designed different experiments that aim to characterize the membrane reaction to desiccation stress of *A. baumannii* as in hospital environments. We focused on two *A. baumannii* strains: the type strain ATCC 19606^{T} and the epidemic strain ACICU (12; 13) because of their different desiccation resistance: ATCC 19606^{T} resulted more sensitive to dehydration compared to ACICU (3). In particular, we combined micro-Raman Spectroscopy (μ–R), Gas Chromatography (GC) coupled to Mass Spectroscopy(MS), Atomic Force Microscopy (AFM) and Fluorescence Recovery After Photobleaching (FRAP), in order to reveal for the first time the bio-physical modification that the membrane of *A. baumannii* undergoes during dehydration.

2. Materials and Methods

2.1. Preparation of bacterial inocula and desiccation conditions

A. baumannii strains ATCC 19606^{T} and ACICU were grown in LB and incubated at 37 ℃ for 18 h. 18 hours-bacterial cultures were sub-cultured

(1:100) in a flask and incubated at 37 ℃ under vigorous shaking (250 rpm). Bacterial cells were sampled after 6 h-incubation by centrifugation (3,000 g x 5 min), washed twice, suspended in H_2O, and diluted to the desired optical density at 600 nm (OD_{600}). Bacterial suspensions in H_2O were air-dried under the laminar flow hood at room temperature and stored in a 16 litres-vacuum bell containing 50 g of silica gel at an average temperature of 20.9 ± 0.6 ℃ and an average relative humidity of 13.00 ± 5 %. Bacterial suspensions were desiccated on electronic-grade silicon (001) wafers for μ-Raman measurements, while glass coverslip (Corning cover glasses, Sigma-Aldrich) and glass slides (Thermo Scientific SuperFrost Microscope slides 76 x 26 mm with 1 mm thickness) were employed for FRAP and AFM analysis, respectively, as detailed in the following sections.

2.2. μ–R Spectroscopy: experimental set-up and data collection parameters

According to the inoculum conditions described above, *A. baumannii* strains ATCC 19606^T and ACICU were diluted in H_2O (OD_{600} = 4). 2.5 μL of bacterial suspensions were spotted on a silicon substrate and the experiment was performed in triplicate. An InVia Renishaw μ–R spectrometer equipped with a Leica DM2700 M confocal microscope has been used to collect unpolarised Raman spectra. A solid-state diode laser source at 532 nm (maximum output power ∼100 mW), was used as excitation pump. A Leica 50X LWD objective allowed focusing the excitation beam down to 1 μm, enabling single bacterial cell analysis. Holographic edge filters gave the high-contrast rejection for elastically scattered component. The anelastic contribution was then dispersed by a diffraction grating (1800 grooves/mm) achieving a spectral resolution of ∼ 1 cm^{-1}. The scattered light is collected

by a 1024 x 256 pixel CCD detector, Peltier cooled (-70 ℃), to reduce the interference of dark counts to a negligible level. The spectra were recorded at room temperature in the wavenumber range 2600–3850 cm^{-1}. The 520.5 cm^{-1} line of the inner silicon standard sample was used to calibrate the spectral energy. WiRE 5.3 software licensed by Renishaw is used for measurements set-up, acquisition and subtraction of systematic errors (i.e. cosmic rays removing).

In order to follow the desiccation process of the samples and optimize the spectral analysis, a 1-min-Raman-timelapse was performed by combining two different set-ups for wet and dry samples. Drops of wet bacterial samples were probed with a surface power density of $6.3 \cdot 10^{10}$ W/m^2, for an exposition time of 1 s for 15 accumulations (acc.), while dried samples with a surface power density of $1.2 \cdot 10^{10}$ W/m^2 for an exposition time of 3 s for 10 acc. These experimental conditions optimize the signal to noise ratio during the whole drying process, avoiding sample degradation and taking into account the drying time, as shown in Figure S1 of Supplementary.

2.3. Lipid extraction and GC-MS analyses

According to the inoculum conditions described above, *A. baumannii* strains ATCC 19606^T and ACICU were suspended in H_2O. 4 mL of these bacterial suspensions were maintained in water or air-dried on a glass Petri dish. At each time point (i.e., 0, 6 and 24 h) desiccated and maintained in water samples were diluted in H_2O to a final $OD_{600} = 3$, centrifuged and after discarding supernatants, bacterial pellets were collected and stored at -20℃. Total lipid extraction and GC-MS analysis were performed as previously described by Lopalco et al. 2017 (14). Lipids were extracted

from frozen bacterial pellets suspended in 200 μL of glacial acetic acid. 5 mL of 1:1 mixture of chloroform and ethanol was added, and samples were vortexed for 3 min. The upper aqueous layer and cell debris at the interface were discarded after centrifugation (10 min at 1,000 x g). The extracts were dried on a rotary evaporator at 30 ℃ before weighing and then dissolved in chloroform (final concentration 10 mg/mL). A chloroform solution of the total lipid extract (about 1 mg) was dried in a rotary evaporator at 30 ℃ and underwent a complete esterification. To a stirred solution of the obtained residue in ethanol was added a large excess of HCl 1.25 M in Ethanol. The reaction mixture was kept under stirring at room temperature for almost 72 h. After the reaction completion, as detected by TLC (Hexane/Ethyl Acetate), the solvents were removed under reduced pressure, the residue was taken up with H_2O (3 mL) and extracted with Hexane (3 x 3 mL). The combined organic layers were dried (Na_2SO_4), filtered, and evaporated under vacuum affording the desire Fatty Acid Ethyl Esters (FAEEs), whose composition was determined as follows.

The GC-MS analyses were carried out on a Shimadzu GC-MS 2010 plus Gas Chromatograph coupled to a Mass Spectrometer Shimadzu GC-MS QP2010 SE. The chromatographic separations were performed using a SLB-5ms column (30 m × 0.25 mm id, film thickness 0.25 μm). The employed GC-MS parameters were: gas carrier (helium) at the constant flow rate of 0.87 mL/min; the injector (split mode) was at 250 ℃; the oven temperature program was 120 ℃ (5 min) to 180 ℃ (3 min) at 20 ℃/min, to 280 ℃ (20 min) at 10 ℃/min.

2.4. AFM: set-up and data analysis

A. baumannii strains ATCC 19606^{T} and ACICU were diluted in H_2O to $OD_{600} = 1$. 20 µL of the bacterial suspension was spotted on a microscope glass (Thermo Scientific SuperFrostTM Microscope slides 76 x 26mm with 1 mm thickness), and dried under laminar flow hood for about 10 minutes. AFM measurements were performed using a Dimension ICON AFM (Bruker, Santa Barbara, CA), operating in PeakForce mode using a ScanAsyst-Air Bruker silicon probe featuring a nominal cantilever elastic constant of 0.4 N/m and a tip with a nominal radius of 5 nm. The AFM images were recorded at a temperature range of 20 - 24 ℃. The force set point was optimized in the 15 - 25 nN range. For each experiment, multiple large scans from 3 µm × 3 µm for single cells to the maximum 98 µm × 98 µm in large scale were scanned in different regions of the glass slide, using a 512 × 512 pixels scanning mash per line in each image. The obtained AFM images were analyzed and processed with the open-source Gwyddion Software (http://gwyddion.net). Multiple images were recorded at each measurement to validate our observations.

The analysed cells were spatially located thanks to a reference mark on the glass cover slip made with a diamond pen in order to measure the same cells at the different time points (0, 1, 6 and 24 h) following dehydration. After finding the targeted cells, they were measured and then stored under controlled condition (subsection 2.1) for the next examination.

2.5. FRAP: Experimental setup and data analysis

A. baumannii strains ATCC 19606^{T} and ACICU were diluted in H_2O to $OD_{600} = 1$ and stained with 1 µg/mL of Texas Red^{TM}-X Succinimidyl Ester (TRSE), ThermoFisher Scientific, to label outer membrane proteins.

Bacterial suspensions were washed with distilled water to remove the excess of dye. An aliquot (20 µL) of the labelled bacterial suspensions was air-dried at room temperature for 24 h. 20 µL of bacterial suspensions maintained in water were poured on a microscope slide coated with 0.5 % agarose to immobilize the cells and to keep them in hydrated conditions. Confocal microscopy inspection was performed with a NikonA1+ equipped with 100 X oil immersion objective (NA 1.4). Two pre-bleach images of each microscopic field were photographed, after which a small portion (circular region of 1 µm of diameter) of cells was circumscribed for bleaching. Each region of interest (ROI) was bleached by exposing the area for 3 iterations (3 s total) to the 405-nm line (LU-N4 laser unit 405, 3.75-mW of power out of fiber). Fluorescence recovery was documented by photographing the cells every 5 min for 90 min after photobleaching. At this time resolution (one frame per 5 min), ROI photofading is minimized. Since we select the minimal ROI allowed (circular region of 1 µm diameter), and *A. baumannii* ACICU cells present $\sim 1\,\mu$m dimensions, bleaching the selected region resulted in the complete bleaching of the cells and total absence of recovery. For this reason, FRAP experiment was performed only on *A. baumannii* ATCC 19606$^{\mathrm{T}}$ cells, owing to their larger size with respect to ACICU (15; 16). Image processing and analysis of fluorescence recovery were performed with the ImageJ program (National Institutes of Health, Bethesda; (17)). Average background value of a cell-free area was subtracted from each image. Photophading correction was performed according to Day et al., 2012 (18). Half time of recovery (t1/2) and mobile fraction % (Mf) were calculated as previously described (18).

3. Results & Discussion

μ–R enables to evaluate the membrane transition from liquid crystalline to gel phase by investigating specific bands, whose intensity ratio varies accordingly to its phase and can be used as Raman marker (9; 19; 20). Drops of bacterial suspension were analysed by 1-min-Raman-timelapses from the deposition up to 5 min after water evaporation, in order to characterize the dehydration process of *A. baumannii*.

Preliminarily, extended range Raman spectra (1100 - 3800 cm^{-1}) of ATCC 19606^{T} and ACICU were acquired (see Figure 1a) in order to identify the most suitable Raman marker. Both strains display similar spectra that can be divided into 5 main regions: the Amide I and Amide II region (∼1600-1690 cm^{-1} and ∼1480-1580 cm^{-1}, respectively) which mainly represent the proteins contribution to the spectrum; the CC stretching region (∼ 1480-1700 cm^{-1}), in which the contributions of both proteins and lipids are present; the CH stretching region (∼2800-3100 cm^{-1}), mainly ascribable to the bacterial membrane lipids; and the water OH stretching region (∼3100-3700 cm^{-1}; as can be seen in Figure 4 of supplementary, the disappearance of the OH band can be used to determine the water evaporation dynamics of the sample (21)) (22; 23; 24; 25; 26; 27; 28). Most of the Raman features of the phase transition belongs to the CC and CH stretching regions (10; 11; 22; 29; 30). We carried out the Raman timelapse on the CH stretching region because the contribution of other bio-molecules, different from membrane lipids, is very low in this part of the spectrum with respect to the CC stretching region, resulting in a site specific analysis.

In order to tag its components, the CH stretching region was deconvoluted

with six Voigt curves (Figure 1b), assigned to: CH_2 symmetric stretching component ($\sim$ 2850 cm^{-1}), CH_2 stretching component ($\sim$ 2870 cm^{-1}), CH_2 asymmetric stretching component ($\sim$ 2915 cm^{-1}), CH_3 symmetric stretching component ($\sim$ 2930 cm^{-1}), CH_3 asymmetric stretching component ($\sim$ 2970 cm^{-1}) and CH stretching component ($\sim$ 3060 cm^{-1}) (22; 26; 27). Our analysis focused on the CH_3 and the CH_2 symmetric stretching bands since their Raman Intensity Ratio (RIR) is influenced by the variations of the lipid aliphatic chain and by the interaction among chains (11; 31).

Interestingly, the RIR of both ATCC 19606^T and ACICU follows a descending sigmoidal trend (Figure 2) that highlights the passage from less packed aliphatic chains of the membranes, ascribable to a liquid crystalline phase, to more packed chains that reduce the stretching motion of the CHs, typical of the gel phase.

The data in Figure 2 were fitted with the following equation:

$$y = A2 + \frac{A1 - A2}{1 + e^{(t-t0)/\tau}} \tag{1}$$

Where A1 and A2 represent, respectively, the asymptote of the starting and finishing plateaus, τ is the time constant and t0 is the abscissa of the point of inflection.

At the beginning of the timelapse, the membranes of both strains are in liquid crystalline phase and the relative RIRs lie in a similar A1 ($\sim$ 7) . At this stage of the timelapse, the Raman spectra display an intense water OH stretching region that drastically reduces at the completion of the water evaporation (see the Supplementary section "Raman - merging data"). At that point, the membranes of the two strains transit to the gel phase with a

similar rate, indeed the two τs are comparable, and the RIRs descend and reach the A2 plateau.

There is a slight difference between the A2 values of the two strains: A2 of ATCC 19606^{T} is 6% lower with respect to ACICU (see Table 1).

Table 1: Fit parameters* of RIR of ATCC 19606^{T} and ACICU and the relative goodness

	ATCC 19606^{T}	ACICU
A1	7,0 ± 0,2	7,0 ± 0,1
A2	4,7 ± 0,1	5,00 ± 0,09
τ	65 ± 16 s	47 ± 9 s
adj. R^2	0,91	0,95

* t0 is omitted since it is irrelevant to the phase transition dynamics

These different values of A2 may suggest the better fitting to dehydration resistance of ACICU with respect to ATCC 19606^{T}. Indeed, the proximity of A1 and A2 of ACICU can be interpreted as a sort of similarity between its gel and liquid crystalline state since they display a similar packing of the CHs. As a consequence, the transition toward the second plateau is faster compared to ATCC 19606^{T}, resulting in a more resistant membrane. In addition, the difference between the two RIRs may also be ascribed to a different lipidic composition along the dehydration process of the cell membranes of ACICU and ATCC 19606^{T}, as discussed in the following paragraphs.

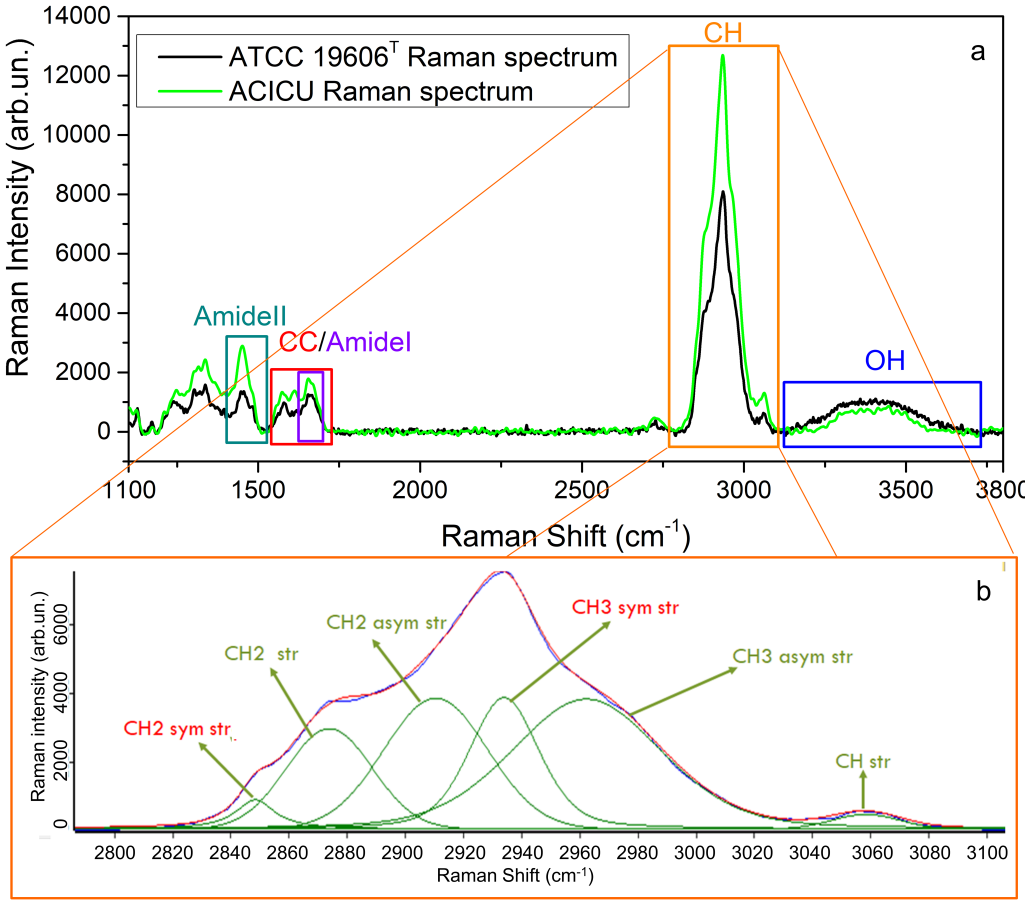

Figure 1: Panel a shows the wide range Raman spectrum (1100 - 3800 cm^{-1}) of *A. baumannii* ATCC 19606^T (black) and ACICU (green) and the identification of spectral regions. The water-green and purple boxes surround the Amide I ($\sim$ 1600-1690 cm^{-1}) and Amide II regions ($\sim$ 1480-1580 cm^{-1}), the red one the CC stretching region ($\sim$ 1480-1700 cm^{-1}), the orange box is the CH region ($\sim$ 2800-3100 cm^{-1}) and the blue box is the OH region ($\sim$ 3100-3700 cm^{-1}) (22; 26; 27). Panel b shows the deconvolution of the CH region of ATCC 16909^T with 6 Voigts curves: the blue curve represents the Raman Spectrum, the red one the relative fit and the green curves are the Voigt curves of deconvolution. Each green curve is representative of a molecular roto-vibration, from low to high frequency, CH_2 symmetric stretching, CH_2 asymmetric stretching, CH_2 asymmetric stretching, CH_3 symmetric stretching, CH_3 asymmetric stretching and CH stretching, the CH_3 and CH_2 symmetric stretching are in red because their intensity ratio is the RIR.

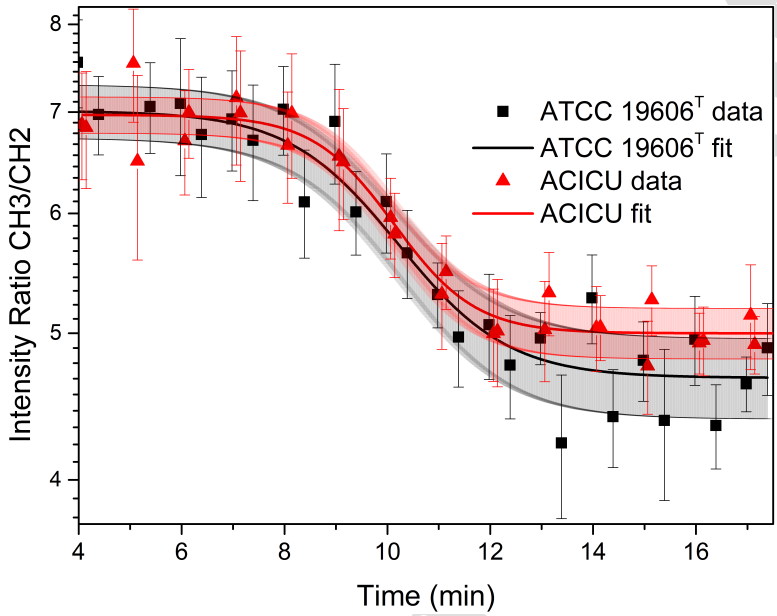

Figure 2: RIR of both ATCC 19606^{T} (black) and ACICU (red). The squares and triangles represent the experimental data, which correspond to the merged data of two timelapses per strain, and the solid lines the relative sigmoidal fit. The data error was computed by using the root mean square error of the CH component deconvolution, while the standard deviation from the mean value of residues was taken as error of the sigmoidal fit.

Figure 3 displays the relative abundance of the observed FAEEs and how it changes during the first 24 h of dehydration for both the *A. baumannii* strains. Non-desiccated ATCC 19606^{T} and ACICU cells present a different lipidic composition of the membrane prior the dehydrating process, since the first one is mainly composed of unsaturated fatty acids. Instead, ACICU is mainly made up of saturated ones.

As the dehydration progresses, the ACICU membrane shows an increase of the relative amount of Ethyl Heptadecanoate and Ethyl (E)-hexadec-9-enoate, maintaining a high amount of saturated fatty acids. On the other hand,

the ATCC 19606^{T} membrane experiences an important change of roles since the fatty acids population of ATCC 19606^{T} changes from an unsaturated to a saturated one. Indeed, there is a reduction of Ethyl (E)-hexadec-8-enoate along with a substantial increase of Ethyl Heptadecanoate, Ethyl (E)-hexadec-9-enoate.

Thus, the GC-MS analysis reveals that the two strains display a similar modification in lipid composition: both strains increase the amount of saturated fatty acids during the first 24 h of dehydration. Moreover, this modification is coherent with the passage from a liquid crystal phase towards a gel phase (as shown above) since saturated fatty acids, because of the less bent lipid chains, tend to increase the packing of the membranes, making them stiffer (4; 6).

Interestingly, this difference may indicate how the two strains fit to dehydration resistance, placing ACICU in a more advantageous situation with respect to ATCC 19606^{T} since the composition of its hydrated membrane is close to the dehydrated one. Thus, ACICU does not have to drastically change its membrane composition as ATCC 19606^{T} does.

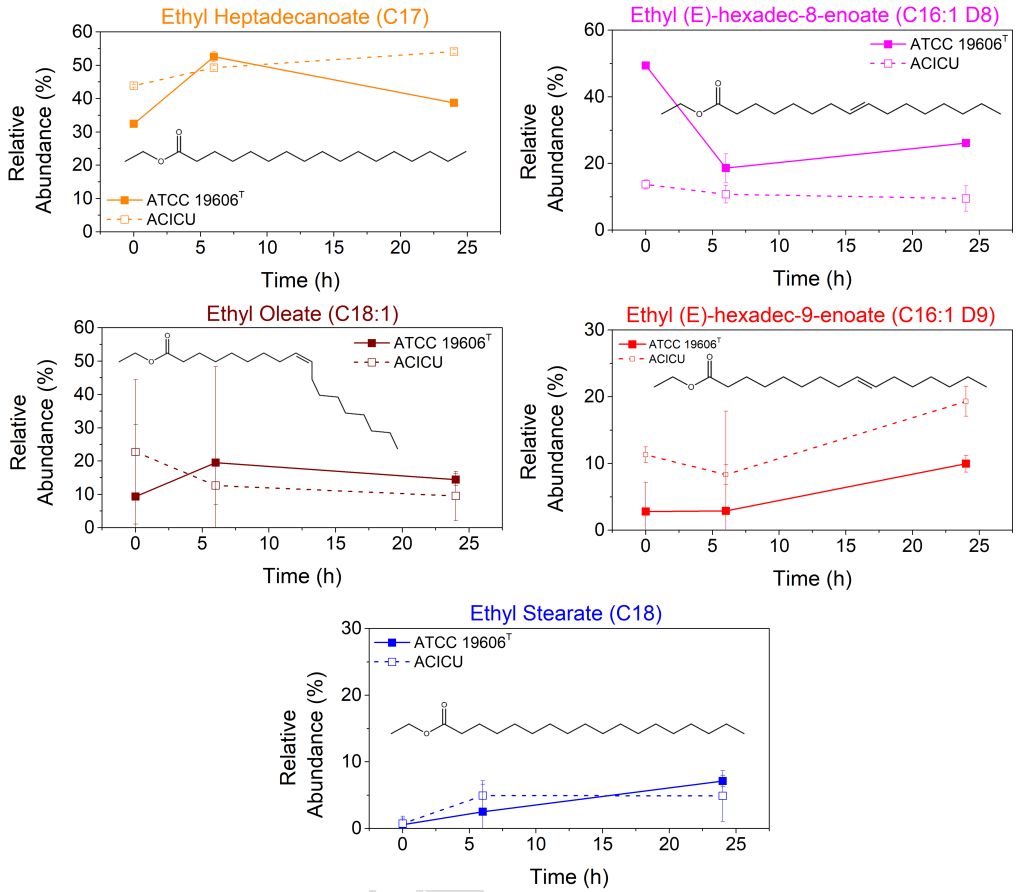

Figure 3: Graphs of the relative abundance of FAEEs released by acid ethanolysis from the total lipid extract throughout a 24 h dehydration and their molecular structure. The data relative to ATCC 19606^{T} are represented with full squares and solid lines, the ones to ACICU with empty square and dashed lines, lines are there only to distinguish between the two strains.

The morphology of ATCC 19606^{T} and ACICU cells was monitored with AFM during the dehydration under room condition for 24 hours, as show in Figure 4. At a first glance, both strains did not show any evident variation in the overall morphology of their cells, only very slight changes were identified

in the membrane curvature and in the aggregation of extracellular materials close to the bacterial cell (yellow arrow in Figure 4a). This deformation in cell membrane curvature could be attributed to its interaction with the closest extracellular materials. Interestingly, this phenomenon was mainly observed in *A. baumannii* ACICU cells, and particularly in single cells or at the boundary cells in clusters.

To have a detailed examination of the morphological response to dehydration of both strains, Figure 4a and b show high magnification (3.5 μm x 3.5 μm) images of dehydrated *A. baumannii* ACICU and ATCC 19606^{T} single cells. It is evident that *A. baumannii* ACICU has a relatively round-shaped cell (length to width ratio ∼1.03, and cell height: 300 nm) featuring depression in the central part of its outer membrane, while ATCC 19606^{T} cells are rod-shaped (length to width ratio ∼2.47, and cell height: 250 nm), displaying a deformation at cellular poles. The depression of the outer membrane observed in both *A. baumannii* strains, is likely the first impact of dehydration process. By analysing the profile of the cells surface and roughness along the plotted dashed line for both strains (Figure 4a1 and b1), very little modifications are noteworthy through time. Both strains display negligible variations of both the height profile and the local surface roughness.

Enlarging the view and analysing clusters of dehydrating bacteria as shown in Figure 5, it is evident that 0 and 1 h dehydrated bacterial cells of each strain are not entirely dried, which is more pronounced in the surrounding region of the bacterial cell cluster, shown by white arrows. After 6 h, water completely evaporates and the bacterial cells of both strains were totally air-dried. Moreover, these cells seem to maintain their overall morphology,

showing little cellular shrinkage and flattening. Indeed, the statistical analysis (Table 2) performed on 30 cells revealed no variation of the cell surface area (S), volume (V) and their ratio (S/V) and, interestingly, the ACICU results are in accordance with those described in Bashiri et al.2021 (15). Moreover, the absence of evident morphological modifications contrasts with other genus reaction to dehydration. As an example, in *E.coli* cells the phase transitions is accompained by a volume contraction, causing holes and cracks in the membrane, which lead to bacterial death (8).

Comparing the two strains, ACICU shows a smaller S/V ratio with respect to ATCC 19606^{T}, and, interestingly, a small S/V ratio has been related to a high resistance to dehydration (15; 32; 33). Moreover, the surface roughness analysis, conducted in the area of 400 X 400 nm on the developed surface, illustrates that at 0 h ACICU cells feature a rougher surface 6 $\pm$ 2 (0 h) than ATCC 19606^{T} 3 $\pm$ 1. This parameter increases for both strains after 6 h of dehydration with ACICU having a higher roughness with respect to ATCC 19606^{T}. It is reasonable to suggest roughness as a marker for the adaptation to drough, as already proposed in Bashiri et al.2021 (15). Putting together the AFM with the μ–R results, it is possible to highlight the morphological and physical modifications that A. baumannii undergoes in order to better adapt to dehydration. In particular, ACICU (the most fitted strain) presents a rougher membrane with a lower S/V ratio along and a quicker phase transition compared to ATCC 19606^{T}.

Table 2: Cellular characteristics and average RMS surface roughness of *A. baumannii* ATCC 19606^{T} and ACICU at different time points of desiccation process

Strain	Time (h)	Cell Surface Area (μm^2)	Cell Volume (μm^3)	S/V (μm^{-1})	Average RMS Roughness* (nm)
ATCC	0	1.0 ± 0.2	0.23 ± 0.05	4.1 ± 0.6	3 ± 1
19606^{T}	1	1.0 ± 0.2	0.23 ± 0.04	4.6 ± 0.6	4 ± 2
	6	0.9 ± 0.1	0.22 ± 0.03	4.2 ± 0.5	8 ± 2
ACICU	0	0.8 ± 0.2	0.25 ± 0.05	3.5 ± 0.5	6 ± 2
	1	0.7 ± 0.1	0.23 ± 0.04	2.8 ± 0.3	8 ± 2
	6	0.7 ± 0.1	0.21 ± 0.03	3.5 ± 0.4	9 ± 2

* Average RMS surface roughness measured over three different 400-nm by 400-nm areas on individual cells. A minimum of 30 cells of each strain was characterized and averaged for roughness analysis.

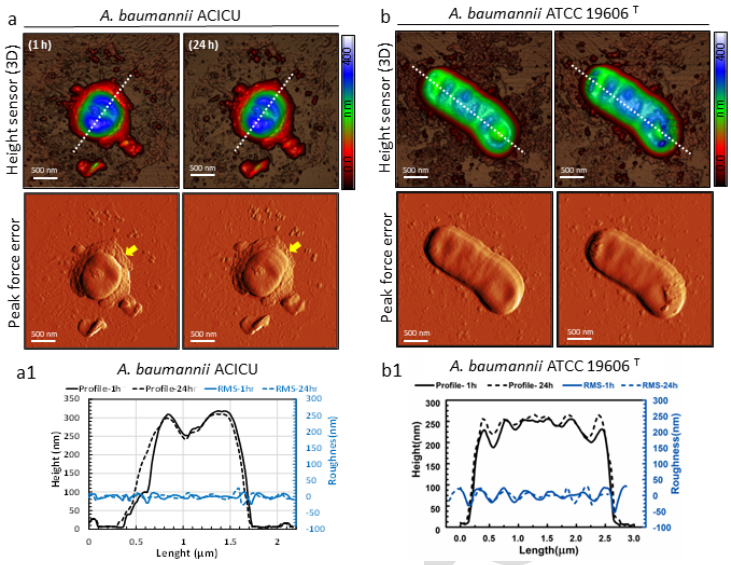

Figure 4: Morphology alterations in *A.baumannii* strains during dehydration. The 3D AFM height and peak force error images of ACICU and ATCC 19606^{T} single cells are shown, respectively in panel a and b. The yellow arrow point to the aggregation of extracellular materials. The profile of cell surface and roughness along the plotted dashed line for both ACICU and ATCC 19606^{T} are represented in panel a1 and b1. AFM height images are set to 400 nm for all bacterial cells.

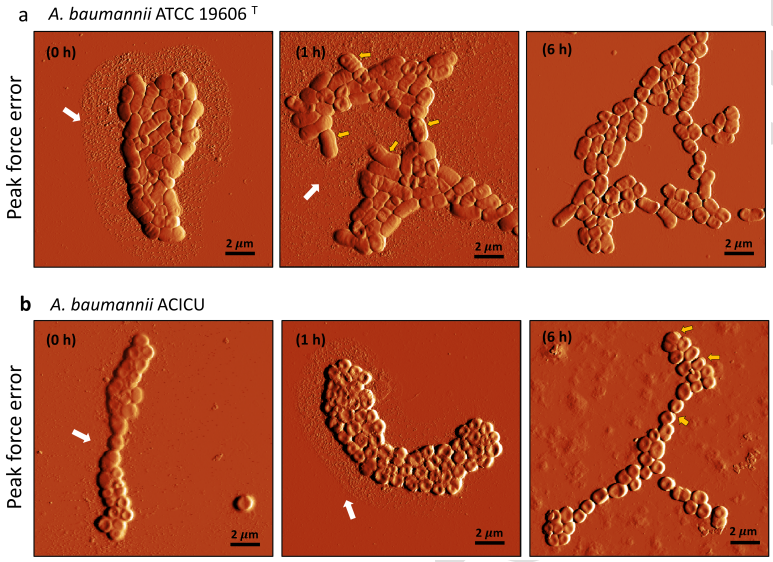

Figure 5: AFM images of *A.baumannii* cell morphology from the early stage of dehydration to air-dried state. Panel a shows the peak force error images for ATCC 19606^{T} and panel b shows the ACICU strains from first minutes of water evaporation at room condition (0 h), within the first hour (1 h), and 6 h. The white arrows show the presence of a water layer surrounding the bacterial cells.

Since during desiccation, bacterial cells face a severe decrease in membrane fluidity as demonstrated by previous μ–R analysis, FRAP technique (Figure 6) was employed to estimate diffusivity modifications that occur due to water loss. In addition, FRAP also estimates the intracellular diffusivity of proteins inside the cells using TRSE as fluorescent reporter. Membrane fluidity and TRSE degree of diffusivity inside the cell were performed on bacterial sample before and after desiccation at different time points (see supplementary materials).

The FRAP experiment was performed in timelapse (Video S1-S2) on desiccated and hydrated cells (i.e., cells immobilized on agarose to keep them in hydrated conditions) of *A. baumannii ATCC* 19606^{T}; in particular, a 1 x 1

μm region of samples was photobleached by laser exposure and photographed every 5 min for 90 min, waiting for the fluorescence recovery.

Hydrated cells easily recovered their fluorescence while those air-dried only partially (Video S1-S2, Figure 6). Such observation is corroborated by the fluorescence intensity curves (Figure 7): cells in both conditions show a fluorescence drop in correspondence of the bleaching action of the laser and only the cells in hydrated condition presented higher and more rapid fluorescence recovery than those desiccated. All these observations were corroborated by assessing the values of M_f and $t_{1/2}$, which were found to be higher and lower, respectively, in hydrated samples compared to desiccated ones (Table 3). These results suggest that the hydrated cells present a more fluid membrane which allows the replacement of bleached molecules with other fluorescently labelled.

Table 3: M_f and $t_{1/2}$ values represent the mean ± standard deviation of FRAP experiments independently performed on three cells for each condition.

	Hydrated	Air-Dried
M_f (%)	36.5 ± 6.9	10.6 ± 2.1
$t_{1/2}$ (min)	15 ± 2.5	27.5 ± 4.1

Moreover, these findings are coherent with the μ–R results for ATCC 19606^T; indeed, it highlights a transition from a fluid liquid crystalline phase towards a stiffer gel phase (Figure 2). Unfortunately, FRAP analysis could not be performed on ACICU samples without bleaching the entire cell because of the coccoidal and smaller dimensions of the strain, demonstrating that the

377 analysis of RIRs is a fast and label-free methodology to evaluate the variations
378 of the state of lipidic membranes that overcame the FRAP technicalities.
379 Thanks to the correlation between the two techniques, we were able to infer
380 a similar trend for the ACICU. In detail, the RIR referred to ACICU present
381 a higher A2, indicating that ACICU is endowed with a higher membrane
382 fluidity than *ATCC* 19606^{T}, despite presenting a faster membrane phase
383 transition.

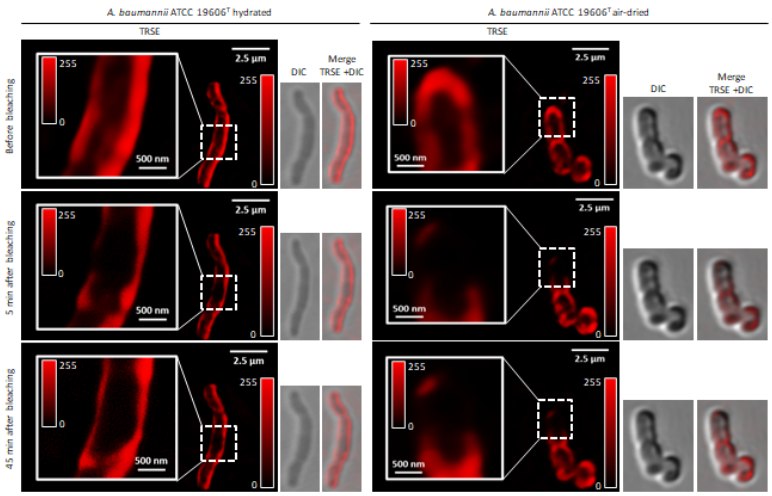

Figure 6: Six representative photograms of videos S1 and S2 are shown, an *A. baumannii* ATCC 19606^{T} cell stained with TRSE, maintained in water (left) and one desiccated (right) for 24 h on a glass coverslip. Images were processed by applying a denoise filter and deconvolution using the Nis_Elements C software to better visualize bacterial membranes. Red scale denotes pixel intensity.

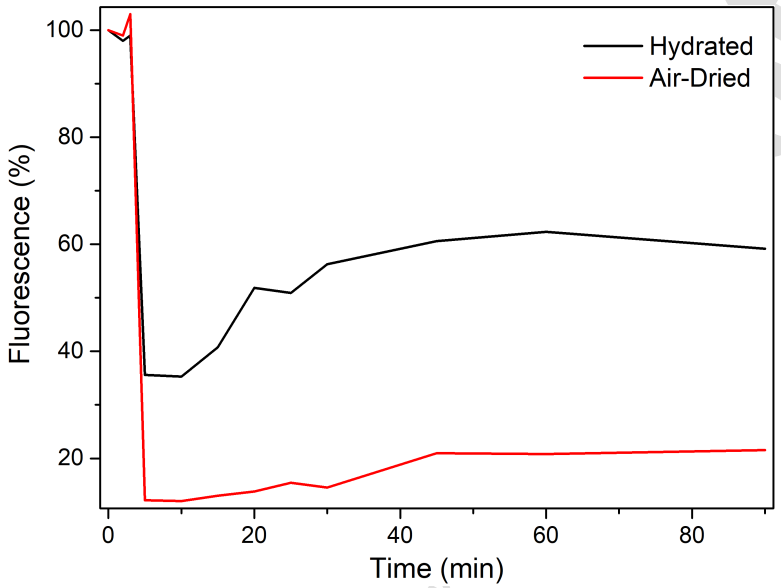

Figure 7: Fluorescence intensity curves of the FRAP experiment. The black and red lines show, respectively, the fluorescence variations of the hydrated and air-dried samples.

4. Conclusions

In this article we exploited a multi-modal approach that combined RS, GC-MS, AFM and FRAP to show for the first time the bio-physical mechanisms that the membrane of *A. baumannii* experiences during dehydration.

Differently from many other Gram-negative bacteria, *A. baumannii* displays a great capacity to withstand dehydration stress, making it a model organism to study desiccation resistance on inert surfaces, as those in hospital environments, (34; 35; 36).

By means of μ–R and FRAP we have shown, that the membrane of both ATCC 19606^{T} and ACICU strains experiences during dehydration a transition from a state where the aliphatic chains of the membrane lipids are loosely

packed to a state where they are closely packed. This modification is due to the phase transition from a liquid crystalline to a gel phase. In particular, ACICU membrane transits slightly earlier than ATCC 19606^{T}s (Figure 2), whose membrane fatty acids change from unsaturated to saturated ones during dehydration. On the contrary, ACICU membrane is mainly composed of saturated fatty acids even before desiccation (Figure 3). Therefore, we conclude that the gel and liquid crystalline phases of ACICU are chemically and bio-physically similar to one another, indicating a better fitting to the dehydration resistance of this strain. Nonetheless, it is not clear yet whether the phase transition is the only factor contributing to the modifications of the membrane composition. To address this point, we are currently investigating the impact of other metabolic processes. Furthermore, AFM characterization (subsection 2.4 and Figure 5) showed an intact membrane, without evident chenges in volume and surface, even 24 h after the dehydration has begun. This proves that the phase transition is not associated to any major membrane modifications for both strains. Consequently, the resistance of *A. baumannii* against drought relies on the fact that the morphology of the cell is not modified by the phase transition of the membrane.

Taken together these results contribute to explain the epidemic success of *A. baumannii* in hospital settings (2), with the reference strain ATCC 19606^{T} being the more susceptible to desiccation compared to the epidemic strain ACICU, in accordance with previous studies (34).

In conclusion, this study provides new insights into the role of membrane composition in the dehydration stress response and shows a substantial decoupling of the phase transitions from evidence of cell lysis of *A. baumannii*

up to 24 h from dehydration since no cracks or holes were found on the surface of the bacterial cells, the membrane appears intact, boosting *A. baumannii* resistance toward dehydration.

All authors contributed to the study conception and design. Samples preparation and FRAP analysis were performed by M.L. and Giu.C., GC-MS by M.L. and T.G., of μ–R by E.F. and M.D.G., of AFM by E.F., S.B. and L.P. The writing of the original draft was performed by E.F. Finally, all authors have read and agreed to the published version of the manuscript.

This work was supported by the Excellence Departments grant from the Italian Ministry of Education, University, and Research (MIUR, Italy) (Art. 1, commi 314-337 Legge 232/ 2016) to the Department of Science, Roma Tre University, and by the PRIN 2017 grant protocol 20177J5Y3P from MIUR to P.V.

The data presented in this study are available on reasonable request from the corresponding author.

We acknowledge the technical support of the LIME laboratory at Roma Tre University.

All the authors declare no conflict of interest.

A. baumannii strains ATCC 19606^{T} and ACICU are available upon request from the authors.

The following abbreviations are used in this manuscript:

μ–R= micro-Raman spectroscopy

GC = gas chromatography

MS= mass spectroscopy

AFM = atomic force microscopy

FRAP =fluorescence recovery after photobleaching

RIR = Raman Intensity Ratio

References

[1] B. Agarwal, R. Karthikeyan, P. Gayathri, B. RameshBabu, G. Ahmed, M. V. Jagannadham, Studies on the mechanism of multidrug resistance of acinetobacter baumannii by proteomic analysis of the outer membrane vesicles of the bacterium, Journal of Proteins and Proteomics 10 (1) (2018) 1–15. doi:10.1007/s42485-018-0001-4.

[2] L. Dijkshoorn, A. Nemec, H. Seifert, An increasing threat in hospitals: multidrug-resistant acinetobacter baumannii, Nature Reviews Microbiology 5 (12) (2007) 939–951. doi:10.1038/nrmicro1789.

[3] M. Giannouli, L. C. Antunes, V. Marchetti, M. Triassi, P. Visca, R. Zarrilli, Virulence-related traits of epidemic acinetobacter baumannii strains belonging to the international clonal lineages i-iii and to the emerging genotypes st25 and st78, BMC Infectious Diseases 13 (1) (2013) 282. doi:10.1186/1471-2334-13-282.

[4] J. H. Crowe, L. M. Crowe, J. F. Carpenter, C. Aurell Wistrom, Stabilization of dry phospholipid bilayers and proteins by sugars, Biochemical Journal 242 (1) (1987) 1–10. doi:10.1042/bj2420001.

[5] K. Brandenburg, U. Seydel, Investigation into the fluidity of lipopolysaccharide and free lipid a membrane systems by fourier-transform infrared spectroscopy and differential scanning calorimetry, Euro-

pean Journal of Biochemistry 191 (1) (1990) 229–236. doi:10.1111/j.1432-1033.1990.tb19114.x.

[6] J. H. Crowe, F. A. Hoekstra, L. M. Crowe, Anhydrobiosis, Annu.Rev.Physiol. (54) (1992) 579–599. doi:10.1146/annurev.ph.54.030192.003051.

[7] N. Paracini, L. A. Clifton, M. W. A. Skoda, J. H. Lakey, Liquid crystalline bacterial outer membranes are critical for antibiotic susceptibility, Proceedings of the National Academy of Sciences 115 (32) (2018) E7587–E7594. doi:10.1073/pnas.1803975115.

[8] L. Beney, Y. Mille, P. Gervais, Death of escherichia coli during rapid and severe dehydration is related to lipid phase transition, Applied Microbiology and Biotechnology 65 (4) (2004) 457–464. doi:10.1007/s00253-004-1574-x.

[9] C. B. Fox, R. H. Uibel, J. M. Harris, Detecting Phase Transitions in Phosphatidylcholine Vesicles by Raman Microscopy and Self-Modeling Curve Resolution, J. Phys. Chem. B 111 (39) (2007) 11428–11436. doi:10.1021/jp0735886.

[10] M. J. L. de Lange, M. Bonn, M. Muller, Direct measurement of phase coexistence in DPPC/cholesterol vesicles using Raman spectroscopy, Chem. Phys. Lipids 146 (2) (2007) 76—-84. doi:10.1016/j.chemphyslip.2006.12.007.

[11] S. Verma, D. F. H. Wallach, Multiple Thermotropic State Transitions in Erythrocyte Membranes, a Laser-Raman Study of the CH-Stretching

and Acoustical Regions, Biochim. Biophys. Acta 436 (1976) 307–318. doi:10.1016/0005-2736(76)90196-6.

[12] I. Artuso, M. Lucidi, D. Visaggio, G. Capecchi, G. A. Lugli, M. Ventura, P. Visca, Genome diversity of domesticated acinetobacter baumannii atcc 19606t strains, Microbial Genomics 8 (1) (2022). doi:10.1099/mgen.0.000749.

[13] M. Iacono, L. Villa, D. Fortini, R. Bordoni, F. Imperi, R. J. P. Bonnal, T. Sicheritz-Ponten, G. De Bellis, P. Visca, A. Cassone, A. Carattoli, Whole-genome pyrosequencing of an epidemic multidrug-resistant acinetobacter baumannii strain belonging to the european clone ii group, Antimicrobial Agents and Chemotherapy 52 (7) (2008) 2616–2625. doi:10.1128/AAC.01643-07.

[14] P. Lopalco, J. Stahl, C. Annese, B. Averhoff, A. Corcelli, Identification of unique cardiolipin and monolysocardiolipin species in Acinetobacter baumannii, Sci Rep. 7 (1) (2017) 2972. doi:10.1038/s41598-017-03214-w.

[15] S. Bashiri, M. Lucidi, D. Visaggio, G. Capecchi, L. Persichetti, G. Cincotti, P. Visca, G. Capellini, Growth phase- and desiccation-dependent acinetobacter baumannii morphology: An atomic force microscopy investigation, Langmuir 37 (3) (2021) 1110–1119. doi:10.1021/acs.langmuir.0c02980.

[16] R. L. Soon, R. L. Nation, P. G. Hartley, I. Larson, J. Li, Atomic force microscopy investigation of the morphology and topography of colistin-heteroresistant acinetobacter baumannii strains as a function of growth

phase and in response to colistin treatment, Antimicrobial Agents and Chemotherapy 53 (12) (2009) 4979–4986. doi:10.1128/AAC.00497-09.

[17] C. A. Schneider, W. S. Rasband, K. W. Eliceiri, Nih image to imagej: 25 years of image analysis, Nature Methods 9 (7) (2012) 671–675. doi:10.1038/nmeth.2089.

[18] C. A. Day, L. J. Kraft, M. Kang, A. K. Kenworthy, Analysis of protein and lipid dynamics using confocal fluorescence recovery after photobleaching (frap), Current Protocols in Cytometry 62 (1) (2012). doi:10.1002/0471142956.cy0219s62.

[19] R. C. J. Spiker, R. W. Levin, Phase transition of phospholipid single-wall vesicles and multilayeres measurements by vibrational raman spectroscopy frequency differences, BBA 433 (3) (1976) 457–468. doi:10.1016/0005-2736(76)90273-X.

[20] A. Csisz´ar, E. Koglin, R. J. Meier, E. Klumppa, The phase transition behavior of 1,2-dipalmitoyl-sn-glycero-3-phosphocholine (DPPC) model membrane influenced by 2,4-dichlorophenol—an FT-Raman Spectroscopy Study, Chem. Phys. Lipids 139 (2) (2006) 115—-124. doi:10.1016/j.chemphyslip.2005.11.005.

[21] T. Corridoni, A. Sodo, F. Bruni, M. Ricci, M. Nardone, Probing water dynamics with oh, Chemical Physics 336 (2–3) (2007) 183–187. doi:10.1016/j.chemphys.2007.06.013.

[22] K. Czamara, K. Majzner, M. Z. Pacia, K. Kochan, A. Kaczora, M. Baran-

skaa, Raman spectroscopy of lipids: a review, J. Raman Spectrosc. 46 (2015) 4–20. doi:10.1002/jrs.4607.

[23] W. E. Huang, R. I. Griffiths, I. P. Thompson, M. J. Bailey, A. S. Whiteley, Raman Microscopic Analysis of Single Microbial Cells, Anal. Chem. 76 (15) (2004) 4452–4458. doi:10.1021/ac049753k.

[24] A. Rygula, K. Majzner, K. M. Marzec, A. Kaczor, M. Pilarczyka, M. Baranskaa, Raman Spectroscopy of Proteins: a Review, J. Raman Spectrosc 44 (2013) 1061–1076. doi:10.1002/jrs.4335.

[25] X. Lu, H. M. Al-Qadiri, M. Lin, B. A. Rasco, Application of Mid-infrared and Raman Spectroscopy to the Study of Bacteria, Food Bioprocess Technol. 4 (2011) 919–935. doi:10.1007/s11947-011-0516-8.

[26] D. Lin-Vien, N. B. Colthup, W. G. Fateley, J. G. Grasselli, Appendix 3 in The Handbook of Infrared and Raman Characteristic Frequencies of Organic Molecules, edn 1, Academic Press, Elsevier, 1991.

[27] M. N. Slipchenko, T. L. Le, H. Chen, J.-X. Cheng, High-Speed Vibrational Imaging and Spectral Analysis of Lipid Bodies by Compound Raman Microscopy, J. Phys. Chem. B 113 (2009) 7681–7686. doi:10.1021/jp902231y.

[28] Z. Movasaghi, S. Rehman, I. U. Rehman, Raman spectroscopy of biological tissues, Applied Spectroscopy Reviews 42 (5) (2007) 493–541. doi:10.1080/05704920701551530.

[29] H. Noothalapati, K. Iwasaki, C. Yoshimoto, K. Yoshikiyob, T. Nishikawa,

M. Ando, H. Hamaguchi, T. Yamamoto, Imaging phospholipid conformational disorder and packing in giant multilamellar liposome by confocal Raman microspectroscopy, Spectrochim. Acta A Mol. Biomol. Spectrosc. 187 (2017) 186–190. doi:10.1016/j.saa.2017.06.060.

[30] B. J. Litman, E. N. Lewis, I. W. Levin, Packing characteristics of highly unsaturated bilayer lipids: Raman spectroscopic studies of multilamellar phosphatidylcholine dispersions, Biochemistry 30 (2) (1991) 313–319. doi:10.1021/bi00216a001.

[31] S. Verma, Low Levels of Irradiation modify lipid domains in Model Membranes: A Laser Raman Study, Radiat. Res. 107 (2) (1986) 183–193. doi:10.2307/3576806.

[32] M. Madigan, J. Martinko, J. Parker, Brock Biology of Microorganisms, Prentice Hall, Upper Saddle River, NJ, 1997.

[33] T. Nyström, Stationary-phase physiology, Annual Review of Microbiology 58 (1) (2004) 161–181. doi:10.1146/annurev.micro.58.030603.123818.

[34] A. Jawad, H. Seifert, A. M. Snelling, J. Heritage, P. M. Hawkey, Survival of acinetobacter baumannii on dry surfaces: Comparison of outbreak and sporadic isolates, Journal of Clinical Microbiology 36 (7) (1998) 1938–1941. doi:10.1128/JCM.36.7.1938-1941.1998.

[35] S. Zeidler, V. Müller, The role of compatible solutes in desiccation resistance of acinetobacter baumannii, MicrobiologyOpen 8 (5) (2019) e00740. doi:10.1002/mbo3.740.

[36] S. Zeidler, V. Müller, Coping with low water activities and osmotic stress in acinetobacter baumannii : significance, current status and perspectives, Environmental Microbiology 21 (7) (2019) 2212–2230. doi:10.1111/1462-2920.14565.

Declaration of interests

☒ The authors declare that they have no known competing financial interests or personal relationships that could have appeared to influence the work reported in this paper.

☐ The authors declare the following financial interests/personal relationships which may be considered as potential competing interests: